Journal of Applied Physics

Assessing the potential of ion beam analytical techniques for depth profiling Li in thin film Li ion batteries

Cite as: J. Appl. Phys. **130**, 125306 (2021); https://doi.org/10.1063/5.0055963
Submitted: 05 May 2021 • Accepted: 08 September 2021 • Published Online: 28 September 2021

Vairavel Mathayan, Kenji Morita, Bun Tsuchiya, et al.

Journal of Applied Physics ARTICLE scitation.org/journal/jap

Assessing the potential of ion beam analytical techniques for depth profiling Li in thin film Li ion batteries

Cite as: J. Appl. Phys. **130**, 125306 (2021); doi: 10.1063/5.0055963
Submitted: 5 May 2021 · Accepted: 8 September 2021 ·
Published Online: 28 September 2021

Vairavel Mathayan,[1,a)] Kenji Morita,[2] Bun Tsuchiya,[3] Rongbin Ye,[4] Mamoru Baba,[4] Marcos V. Moro,[1] and Daniel Primetzhofer[1]

AFFILIATIONS

[1]Department of Physics and Astronomy, Uppsala University, Box 516, SE-75120 Uppsala, Sweden
[2]Department of Research, Nagoya Industrial Science Research Institute, 2F Noah Yotsuya Building, 1-13, Yotsuyatori, Chikusa-ku, Nagoya 464-0819, Japan
[3]Faculty of Science and Technology, Meijo University, 1-501, Shiogamaguchi, Tempaku-ku, Nagoya 468-8502, Japan
[4]Faculty of Science and Engineering, Iwate University, Ueta-4-3-5, Morioka, Iwate 020-8551, Japan

[a)]**Author to whom correspondence should be addressed:** vairavel.mathayan@physics.uu.se

ABSTRACT

Depth resolution and probing depth for Li in lithium thin film batteries achievable using different ion beam analytical techniques were investigated. Experiments using protons for nuclear reaction analysis, He ions for time-of-flight (TOF) energy elastic recoil detection analysis (ERDA) in transmission geometry, as well as He and Li ions for coincidence ERDA in transmission geometry are performed. Experimental results are compared in terms of the obtained Li concentration in the separator layer. In coincidence ERDA experiments, significant loss of Li–Li and He–Li coincidence counts was observed due to multiple scattering of recoiled/scattered particles in the battery sample. The ideal achievable Li depth resolution was calculated for the ion beam techniques. A depth resolution of 750, 1030, 310, and 510×10^{15} atoms/cm^2 could be achieved in the Nb_2O_5 cathode by nuclear reaction analysis (NRA) using 2 MeV H, TOF-ERDA using 8 MeV He, and coincidence ERDA using 8 MeV He and 8 MeV Li ions, respectively, upon optimization of the experimental setup. While a depth resolution of 120×10^{15} ions/cm^2 could be achieved for Li by conventional TOF-ERDA using an solid-state detector energy detector and light primary ions such as O under gracing incidence, TOF-ERDA experiments are found to produce significantly higher beam damage in batteries than other techniques. The beam damage in NRA and coincidence ERDA as performed in this study is estimated to be of the order of 10^{-4} dpa.

I. INTRODUCTION

Methods capable of depth profiling light species are highly relevant in research within plasma–surface interaction,[1] on energy materials such as metal hydrides,[2] and within the steadily increasing activities on high-density energy storage.[3,4] Different from present commercial Li ion batteries using organic electrolytes as a separator, intensive research is focusing on all solid-state batteries. This design is safer and, in the form of thin film batteries, offers a promising option for powering wearable electronics, medical implants, and integration to microelectronics. However, some challenges remain for thin film batteries to enter the commercial market, in particular, high interfacial resistance at interfaces of electrolyte and electrodes limiting power and rate performances.[5,6] To address this issue and subsequently improve battery design and performance, *in-operando* monitoring of Li and other light element mass transport through interfaces with nm scale depth resolution are of vital importance.

Neutron based techniques have been used for *in-operando* characterization of Li ion batteries. Neutron powder diffraction has been used to study Li_xFePO4 cathode materials and metastable phases of Li_xFePO4 have been studied *in situ*.[7–9] *In situ* x-ray photoemission spectroscopy has revealed the various decomposition

products Li_3P, Li_3N, Li_2O, and Li_3PO_4 from Li/LIPON interface during battery operation.[10] Also, microscopies, such as TEM, SEM, and AFM, have been used for Li ion battery research,[11] i.e., Liu *et al.* have studied the composition of Al nanowires by *in situ* TEM and found the formation of Al–Li–O glass during cycling.[12] Recently, also various ion beam analytical techniques have been used for the characterization of Li ion batteries. *In situ* nuclear reaction analysis (NRA) and *in situ* elastic recoil detection analysis (ERDA) were used for depth profiling Li in Li ion batteries.[13–15] Using a coincidence ERDA approach, *in-operando* depth profiling of a full battery stack using Li and He primary beams was demonstrated.[16] The coincidence ERDA technique can, in principle, be applied for depth profiling of any light element in thin foils; also, H depth profiling[17,18] and C depth profiling[19] have been reported by measuring H–H and C–C scattering in coincidence experiments.

In this study, NRA, TOF-ERDA, and coincidence ERDA techniques are compared in terms of achievable depth resolution, ion beam damage, and penetration depth in thin film battery (TFB). Depth profiles of Li are extracted by NRA, transmission ERDA by TOF-E detector, coincidence ERDA by 8 MeV $^4He^{2+}$ ions, and 8 MeV $^7Li^{2+}$ ions in a thin film battery with a total stack thickness of 3.6 μm. The experimental data are complemented by calculations of the achievable depth resolution and resulting damage profiles.

II. EXPERIMENTAL DETAILS

The thin film battery employed for the experiments was prepared by depositing LMO, LIPON, NbO, and Ti layers on a 2 μm Ti self-supporting foil using magnetron sputtering.[20] First, the depth profile of ^7Li in thin film Li ion battery was measured by NRA. In NRA, 2 MeV H ions were directed to the bottom Ti substrate of TFB in normal incidence and the α particle from $^7Li(p,\alpha)^4He$ nuclear reaction was recorded using a silicon solid-state detector (SSD) with 30 keV energy resolution kept at 170° scattering angle (Fig. 1). The NRA spectrum was simulated using the SIMNRA7.02 software package to extract the ^7Li depth profile of sample.[21] Next, the coincidence ERDA technique[22] was employed using 8 MeV $^4He^{2+}$ and 8 MeV $^7Li^{2+}$ ions for specific detection of Li from the sample.[23] In these experiments, circular ion beams with 1 mm diameter were directed in normal incidence on the Ti substrate side of the TFB. For a primary beam of 8 MeV $^4He^{2+}$, forward scattered ^4He and recoiled Li were detected by SSD1 and SSD2 kept at scattering angle of 60° and 45°, respectively, as shown in Fig. 1. The angle of SSD1 and SSD2 was chosen from trivial scattering kinematics.[23] A coincidence time acceptance window of 1 μs was used. The ion beam flux was set to approximately 5×10^{10} ions cm^{-2} s^{-1}. For 8 MeV $^7Li^{2+}$-ions as a primary beam, scattered and recoiled Li was detected by SSD1 and SSD2 with the scattering angle of 45°. Again, a coincidence time acceptance window of 1 μs was used. The ion beam flux was set to approximately 5×10^{10} ions cm^{-2} s^{-1}. The detector resolution of both SSD1 and SSD2 is approximately 30 keV for both He and Li.

The Li depth profile was also measured by TOF-ERDA.[24] In the TOF-ERDA experiments, 8 MeV $^4He^{2+}$ primary ions were again directed on the Ti substrate side and the time of flight and energy of forward scattered He and recoiled particles were measured in coincidence using a time of flight telescope and a gas ionization chamber (with 150 keV resolution for Li), respectively. The whole assembly was kept at a scattering angle of 45° as shown in Fig. 1. Energy and TOF coincidence events permit to discriminate Li from other scattered/recoiled particles and Li depth profile was measured. Experimental Li energy profiles from Li–Li, He–Li, and TOF-E coincidence ERDA spectra were simulated by SIMNRA7.02 to quantify the Li depth profile. The achievable depth resolution of Li in the NRA and coincidence ERDA experiments was calculated using RESOLNRA,[25] and the beam damage was estimated from The Stopping and Range of Ions in Matter (SRIM) calculation.[26]

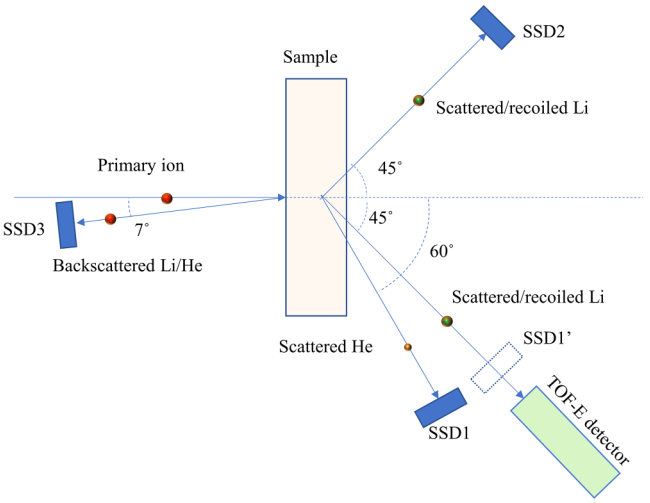

FIG. 1. Top view of a sketch of the experimental setup used for depth profiling of Li in thin film battery stacks. Silicon surface-barrier detectors (SSDs) were used for coincidence ERDA and RBS/NRA experiments. SSD1 and SSD2 were used for He–Li coincidence ERDA. SSD2 and SSD1 at 45° (SSD1′) were used for Li–Li coincidence ERDA. Transmission ERDA data were recorded by a TOF-E detector coupled with a gas ionization chamber. SSD3 was used to measure RBS on the sample.

III. RESULTS AND DISCUSSION

The nominal thickness and composition of the TFB-stack is Ti(50 nm)/Nb_2O_5(90 nm)/$Li_3PO_{4-x}N_x$(940 nm)/$LiMn_2O_4$(560 nm)/Ti(2 μm), which is in very good agreement with results from Rutherford backscattering spectrometry (RBS).[16] The intended composition is approximately $x \sim 0.2$ in $Li_3PO_{4-x}N_x$. The NRA spectra measured in the TFB are shown in Fig. 2. Counts from alpha particles originating from the $^7Li(p,\alpha)^4He$ nuclear reaction can be identified in the spectrum at energies ranging from 6.5 to 7.5 MeV, virtually free from any background (the energy of ^4He from the nuclear reaction is 7.496 MeV at the scattering angle of 170° in the laboratory frame of reference).[27] Additional counts from alpha particles originating from the $^{31}P(p,\alpha)^{28}Si$ nuclear reaction can also be seen at energies ranging from 2 to 3 MeV on top of a small contribution of pileup counts. In the SIMNRA7.02 simulation, NRA cross sections from Refs. 27 and 28 were used for Li

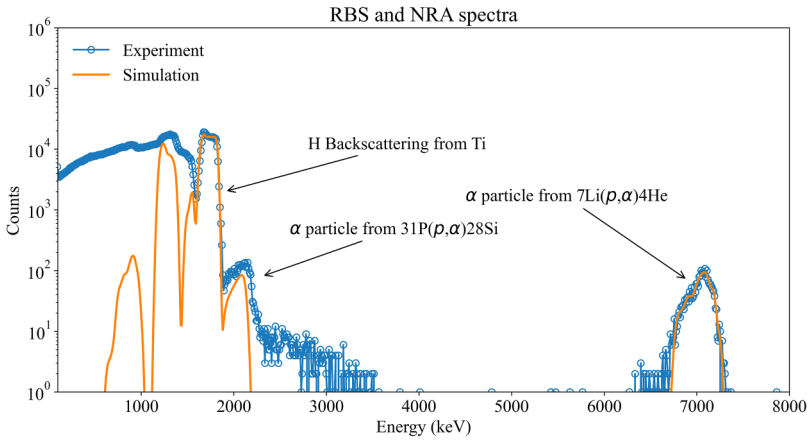

FIG. 2. Experimental and simulated RBS/NRA spectra of thin film battery measured using 2 MeV $^1H^+$ primary ions in normal incidence to the sample surface. The NRA spectrum is normalized using the yield of scattered particles from the Ti substrate.

and P, respectively. Non-Rutherford cross sections were employed for an energy higher than 1.8 MeV for scattering from Ti. The RBS signal from the Ti substrate was used to normalize the NRA spectrum. The resulting areal density of Li is $5880 \pm 120 \times 10^{15}$ atoms/cm^2 in the whole battery stack. The total Li areal density in the battery sample is found to be conserved within the accuracy of the methods when the battery is charged/discharged and the Li is transported through different layers. The Li concentration is measured to be 14%–28% in LIPON layers which is less than the nominal value of 37.5% due to overcharging and discharging.

Figure 3(a) shows the experimental coincidence ERDA spectrum measured by 8 MeV Li ions in the battery sample. A well separated Li–Li coincidence signal is obtained. To compensate for effects from small deviations from scattering/recoiling by 45°, the energy of SSD1 and SSD2 is averaged (E1 + E2)/2, and the Li–Li coincidence spectra are projected to average energy. The energy-averaged Li transmission ERDA spectra are shown in Fig. 3(b). In the simulation of the energy profile for recoiled/scattered Li, Rutherford scattering cross sections are used as these values are comparable to experimental Li–Li Mott cross sections observed by Bachmann *et al.*,[29] Pinsonneault and Blair,[30] and Norbeck *et al.*[31] in the relevant energy range. Results show, however, that the experimental yield is around 17 times lower than those predicted from the simulations. This loss of Li counts can be understood from the significant influence of multiple scattering, which is significantly deteriorating the likelihood of coincidence detection, for the employed detector solid angle. Further, to illustrate the effect of the angular spread of the analyzing ion beam, angular profiles of 8 MeV Li ions transmitted through a TFB as employed in our experiments are simulated by SRIM and are shown in Figs. 4(a) and 4(b). The full width half maximum (FWHM) of the angular distribution of transmitted ions was calculated to be around 1°.

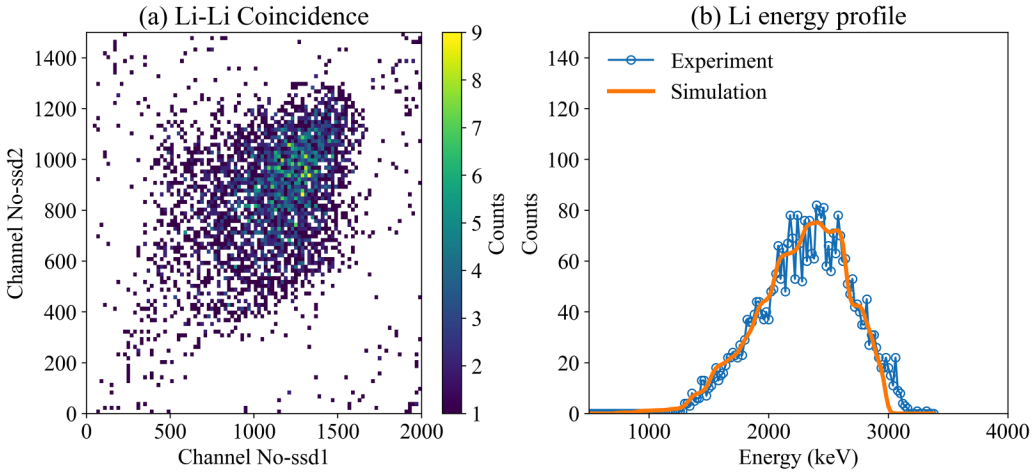

FIG. 3. (a) Coincidence ERDA spectra of forward scattered/recoiled particles from two SSD detectors kept at 45°. (b) Experimental and simulated recoiled Li energy profile by Li–Li coincidence ERDA. The simulated Li energy profile was fitted to the experiment by employing a multi-layer target model and fixing the total Li areal density to the value obtained by NRA.

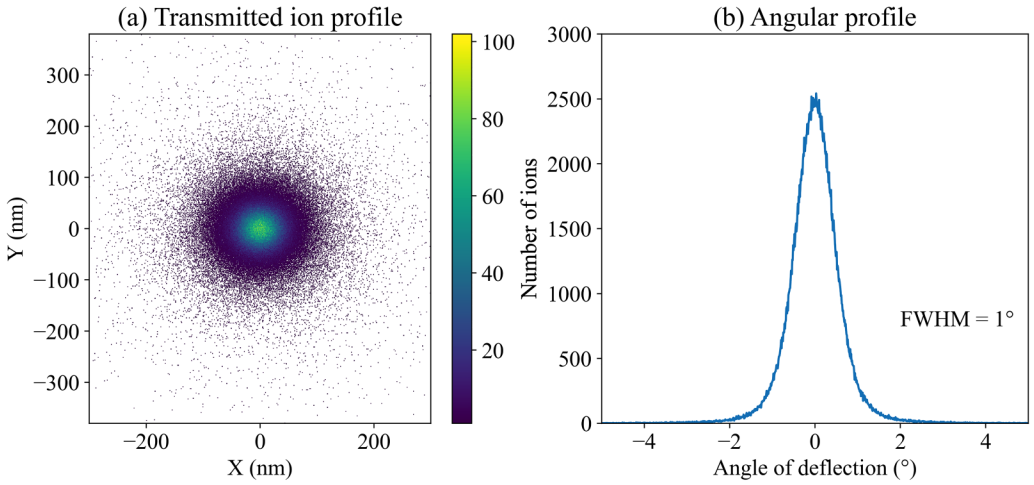

FIG. 4. (a) Lateral profile of Li ions with 8 MeV primary energy transmitted through the thin film battery. (b) Deflection angle of ions transmitted through a simulated battery stack. The estimated full width at half maximum is around 1°.

This value can be compared to the acceptance angle of SSD1 and SSD2 in our experiment being equivalent to 3.2°. Based on the experimental geometry and the energy transfer in the close collision, even more pronounced angular straggling can be expected for the outgoing scattered particles and recoils, and the observed loss in the signal can be well understood. Thus, to fully quantify results from coincidence ERDA, a quantification of the integral Li concentration from, e.g., NRA is essential. A possible alternative would be a full Monte Carlo calculation of the experimental geometry to estimate straggling losses.[32,33] Figure 3(b) shows the experimental coincidence ERDA spectrum along with a simulation. For the simulation, layer thickness and composition as obtained from RBS were used and the Li concentration was adjusted for every layer in a multilayer model to match the experimental data while the integral Li areal density was fixed in the whole battery stack to the value determined from NRA. As a result, the obtained Li concentration is found to vary from 23 to 40 at. % in LIPON layers, which is in good agreement with expectations.

Coincidence ERDA was also performed by 8 MeV $^4He^{2+}$ ions for comparison. The coincidence ERDA spectrum is shown in Fig. 5(a). The spectrum has a well separated He–Li coincidence signal. The He–Li coincidence ERDA spectrum shown in Fig. 5(a)

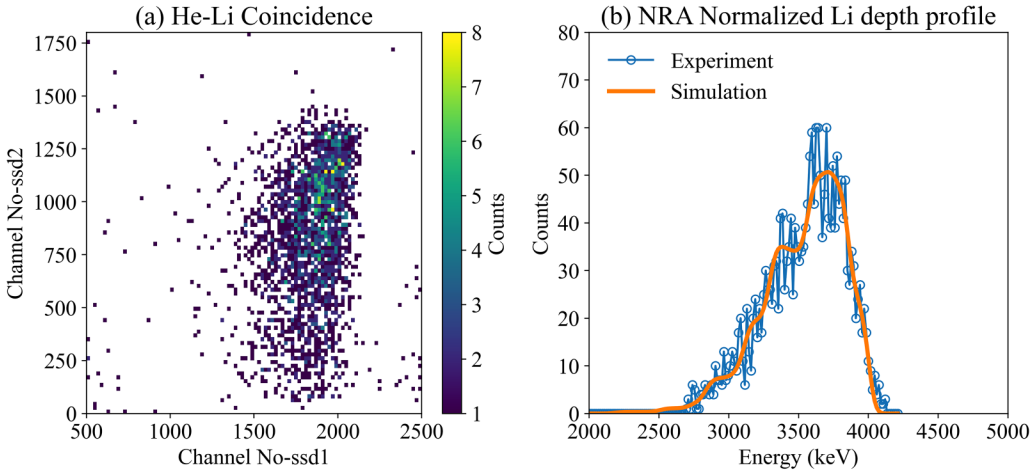

FIG. 5. (a) Coincidence ERDA spectra of forward scattered/recoiled particles from two SSD detectors kept at 45° and 60°. (b) Experimental and simulated Li depth profile by He–Li coincidence ERDA. The simulated Li energy profile was fitted to the experiment by employing a multi-layer target model and fixing the total Li areal density to the value obtained by NRA.

is projected on the y axis and the scattered He spectrum is obtained and shown in Fig. 5(b). Again, the experimental Li signal was found lower than that expected from simulations. Note again, that cross sections were assumed to be Rutherford in absence of known published values. Moreover, also in He–Li coincidence measurements, a similar loss in coincidence events is expected due to finite angular spread of He ions and multiple scattering of scattered/recoiled particles. Again, the experimental Li energy profile is simulated assuming a target model using SIMNRA7.02. In the target model, the composition of Li was adjusted in all the layers while the total areal density of Li was fixed to the total areal density obtained by NRA. The optimized simulation for the Li energy spectrum is shown in Fig. 5(b). In the simulation, LMO and LIPON thin film layers in the sample were further divided into multiple layers and again fitted to the experimental data by adjusting their respective Li concentration. From this fitting procedure, the Li concentration was found to vary from 17% to 33% in the LIPON layer.

The TOF-ERDA spectrum obtained by 8 MeV $^4He^{2+}$ ions is shown in Fig. 6(a). As apparent, in the TOF-ERDA spectrum, Li recoils are well separated from He ions scattered in the TFB. Additionally, the signal of N and O recoils from the battery can be also seen. The Li depth profile was obtained by projecting the Li signals to the energy-axis in the TOF-ERDA spectrum. Also, the sensitivity for Li is found lower in the employed TOF-E ERDA setup.[34] One can normalize the TOF-ERDA spectra via the total Li areal density obtained by NRA. The NRA-normalized experimental and simulated Li depth profile is shown in Fig. 6(b). The resulting concentration profile is similar to NRA but the limited depth resolution is apparent. Figure 7 shows Li depth profiles derived from the different ion beam analysis techniques reported here. A significant amount of Li is present close to or in the Ti substrate that is associated with overcharging the battery with +5 V and discharging with −5 V, respectively. In all the measurements, Li depth profiles look rather similar, in particular, when considering the method dependent depth resolution, which we discuss in the following paragraph.

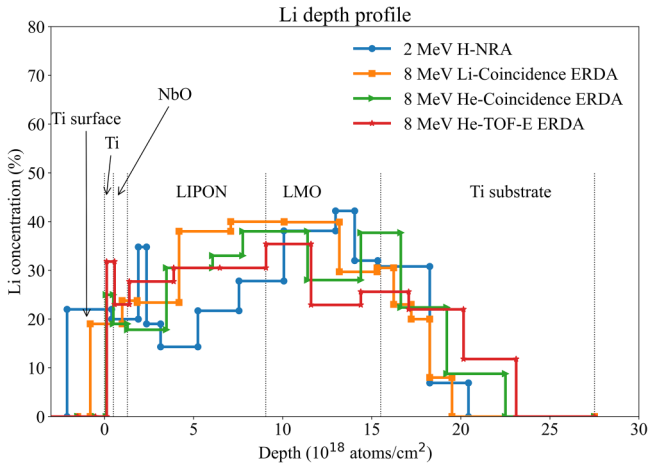

FIG. 7. Li depth profile in the target model derived from SIMNRA7.02 simulations for the employed ion beam analytical techniques (i) NRA using 2 MeV H, (ii) coincidence ERDA by 8 MeV Li, (iii) coincidence ERDA by He, and (iv) TOF-ERDA using 8 MeV He ions.

The achievable depth resolution for Li-profiling at the Nb_2O_5 layer (with 200×10^{15} Li/cm^2) was simulated for optimized detector resolutions and is shown in Fig. 8. The achievable resolution is 750×10^{15} atoms/cm^2 for NRA using 2 MeV H ions with 45° grazing incidence at the top Ti side. The best depth resolution achievable is 310 and 510×10^{15} atoms/cm^2 for coincidence ERDA

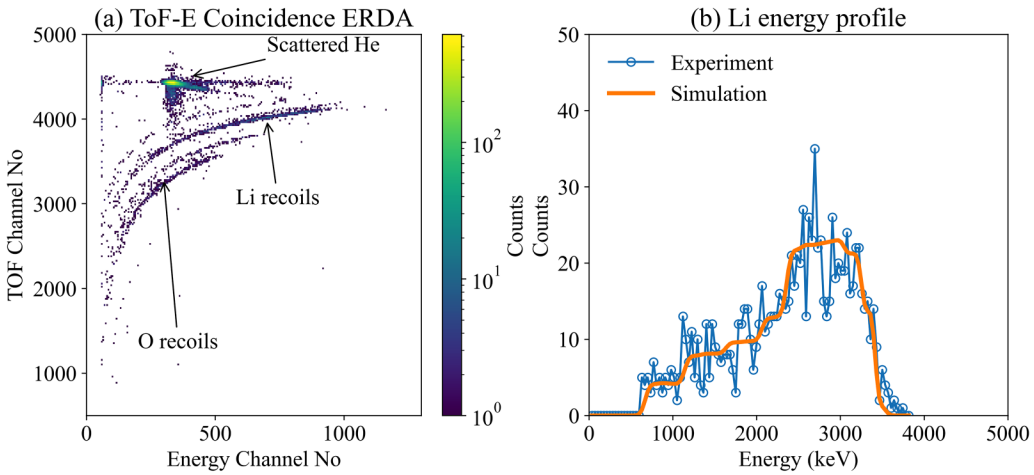

FIG. 6. (a) TOF-ERDA spectra of battery in transmission geometry measured by 8 MeV He ions. (b) Experimental Li energy profile obtained by TOF-E ERDA spectra and the simulated Li energy profile. The simulated Li energy profile was fitted to the experiment by employing a multi-layer target model and fixing the total Li areal density to the value obtained by NRA.

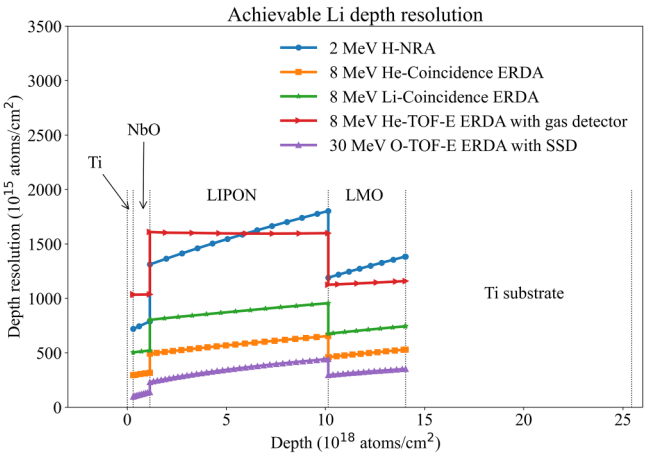

FIG. 8. Depth resolution for Li achievable in the battery stack by NRA, He–Li coincidence ERDA, Li–Li coincidence ERDA, and transmission TOF-ERDA using a gas ionization chamber. Li depth resolution for transmission TOF-ERDA coupled with an SSD detector using 8 MeV He ions and conventional TOF-ERDA by 30 MeV O ions is shown for comparison.

by 8 MeV He ions and 8 MeV Li ions, respectively. Despite the higher electronic energy loss of Li in comparison to He ions in the battery sample, the lower energy loss straggling of He ions results in a better depth resolution for He compared to Li ions. The depth resolution contribution from energy straggling is 220 and 430×10^{15} atoms/cm^2 at Nb_2O_5 for 8 MeV He and Li ions, respectively. Assuming an optimized detector resolution of 120 keV for a gas ionization chamber, the achievable depth resolution is 1030×10^{15} atoms/cm^2 for TOF-ERDA in transmission geometry using 8 MeV He ions. Replacing the gas ionization chamber by an SSD energy detector with 25 keV energy resolution for recoiled Li, the depth resolution was calculated for the same transmission TOF-ERDA experiment using 8 MeV He ions to be similar to coincidence ERDA by 8 MeV He ions. Conventional TOF-ERDA can feature very good depth resolution in the near surface region but depth resolution in subsurface layers will be rapidly degrading, due to the rather gracing incidence angle and/or detection geometry.[35] When used to depth profile parts of a TFB, conventional TOF-ERDA employing 36 MeV iodine primary ions may be capable of depth profiling approximately 1.3 μm with very limited depth information from deeper structures. With an appropriate choice of primary ions, primary ion energy, and angle of incidence, the depth resolution and penetration depth can, however, be improved. For conventional TOF-ERDA with SSD detector, the best achievable resolution, according to RESOLNA, is around 60×10^{15} atoms/cm^2 at Nb_2O_5 layer for 5 MeV O with 67.5° gracing incidence. The penetration depth, however, is limited to 700 nm but could be used to depth profile Li at the LIPON/Nb_2O_5 interface. However, with increasing primary O ion energy, for example, to 30 MeV, the whole battery stack can potentially be probed by conventional TOF-ERDA. The achievable Li depth resolution is 120×10^{15} atoms/cm^2 at the Nb_2O_5 layer (shown in Fig. 8), which is better than the coincidence ERDA by 8 MeV Li ions (310×10^{15} atoms/cm^2). Note that the present calculations do not account for the deteriorating effect due to geometrical straggling, which is expected to lead to a rapidly degrading depth resolution for larger depth associated with the non-normal incidence. Furthermore, the beam damage due to 30 MeV O is nearly ten times higher than that of 8 MeV He and Li ions used in coincidence ERDA (see Fig. 9 and the discussion in Sec. IV). Finally, the time-of-flight telescopes commonly employed for TOF-ERDA feature small solid angles[24,36,37] requiring long time irradiation and high integral fluences to get analyzable statistics of Li recoils. Altogether, the TOF-ERDA experiments using 30 MeV O ions create deteriorating effects in samples due to beam damage and heating and make them unsuitable for *in-operando* experiments.

Considering the lateral resolution, the present experiments were performed using circular ion beams with typically ~1 mm diameter, and imaging is not feasible. Smaller beams have been employed *ex situ* on cross sections of thin film batteries.[38] If a micro- or nanobeam is used in the approach discussed here, 3D mapping of the Li concentration in a battery could be performed with micro/nanometer resolution.

In general, the use of ion beams as probes may cause battery degradation due to, e.g., ion implantation, beam heating, or direct beam induced damage. However, in NRA and coincidence ERDA experiments, degradation due to ion implantation is considered to be rather negligible as most of the probing ions are transmitted through the samples. As an accessible parameter, structural degradation or defect formation will be clearly associated with displacements of atoms from equilibrium sites. To calculate the displacements per atom (dpa) values, the ion beam damage was simulated using full cascade SRIM calculations[26] with a displacement threshold of 25 eV for all atoms, and the number of atomic displacements due to ion beam was calculated for identical ion fluence of 10^{16} ions/cm^2 for comparison and shown in Fig. 9.

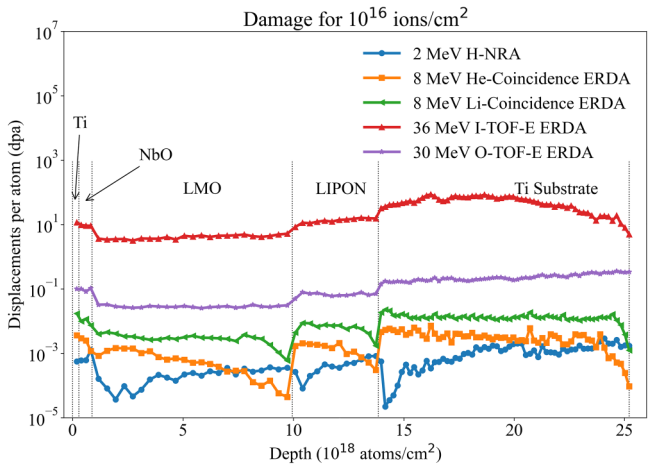

FIG. 9. Damage produced by beams of 2 MeV H, 8 MeV He, and 8 MeV Li ions with normal incidence for identical ion fluence of 10^{16} ions/cm^2. The damage produced by 30 MeV O and 36 MeV I ions incident under 67.5° incidence angle with respect to the sample normal is shown for comparison.

TABLE I. Comparison of beam induced damage and achievable depth resolution for different ion beam analytical techniques capable of Li depth profiling in thin film battery stacks. Predictions are obtained using SRIM and RESOLNA, respectively. For details, see text.

Technique	Average damage in LIPON for 10^{16} ions/cm^2 (10^{-4} dpa)	Depth resolution at Nb_2O_5 (10^{15} atoms/cm^2)
NRA	2.5	750
Coincidence ERDA using 8 MeV Li ions	26	510
Coincidence ERDA using 8 MeV He ions	5.5	310
TOF-ERDA using 8 MeV He ions	5.5	1030

The ion beam damage was also calculated for conventional TOF-ERDA using 36 MeV I and 30 MeV O ions and shown in Fig. 9 for comparison. The average ion beam damage, in LIPON layer, for 10^{16} ions/cm^2 of 2 MeV H, 8 MeV He, and 8 MeV Li ions are 2.5, 5.5, and 26×10^{-4} dpa, respectively, nearly three orders of magnitude lower than for 36 MeV I ions (3.7 dpa). For comparison, the average beam damage in the LIPON layer is 2.5×10^{-2} dpa for 30 MeV O ions with gracing incidence of 67.5°. Thus, in the present coincidence, ERDA experiments, using 8 MeV He or Li primary ions, the integral number of atomic displacements during ion beam irradiation is small in the battery, comparable to values from NRA. Still, during operation, the displaced atoms may cause, to a certain extent, postirradiation degradation of the battery. However, coincidence ERDA combines the advantages of moderate damage and superior depth resolution. Thus, analysis by coincidence ERDA ion beam appears attractive for *in-operando* quantification of Li and other light elements in TFB.

In the experiments of He–Li coincidence ERDA, the energy resolution could be affected due to angular deviations of transmitted ions and the finite acceptance angle of detectors. However, in Li–Li coincidence ERDA, the small angular deviations are partially canceled due to energy averaging of each coincidence event. Thus, Li–Li scattering has advantage of having a low effect on Li depth resolution due to small angular deviations. The solid angle of detectors could be increased in Li–Li and He–Li coincidence ERDA which, as an additional benefit, would further reduce the beam damage. For quantification from stand-alone coincidence ERDA, Monte Carlo programs, which account for depth-resolved coincidence losses due to multiple scattering, could be used. To the best of our knowledge from commonly available programs, only CORTEO[33,39] would be capable of simulating coincidence ERDA spectra. However, this program is limited exclusively to symmetric coincidence measurements, with limited possibilities for the end user to modify many necessary parameters.

IV. SUMMARY

We demonstrate depth profiling Li by NRA, coincidence ERDA by 8 MeV He and Li ions, and TOF-ERDA by 8 MeV He ions in a 3.6 μm thick Ti/LMO/LIPON/NbO/Ti battery. Loss of coincidence counts was predicted in transmission TOF-ERDA and coincidence ERDA experiments with 8 MeV $^7Li^{2+}$ and 8 MeV $^4He^{2+}$ ions due to angular deviations of incidence ion beams and multiple scattering. Thus, integral Li concentrations should be measured prior to TOF-ERDA and coincidence ERDA experiments. TOF-ERDA and coincidence ERDA spectra were normalized by total Li areal density measured by NRA, and Li was quantified in LIPON layers by simulating the experimental Li energy profile. The NRA, TOF-ERDA, and coincidence ERDA experiments predict comparable Li concentrations in LIPON and other layers of battery within experimental uncertainties (shown in Fig. 7). Ion beam damage and achievable depth resolution were calculated and compared (shown in Table I). The damage is of the order of 10^{-4} dpa in all the methods; thus, it may produce only postirradiation degradation during operation. The depth resolution of 310 and 510×10^{15} atoms/cm^2 could be achieved by coincidence ERDA using 8 MeV He and 8 MeV Li ions upon optimization of the experimental setup. For comparison, conventional TOF-ERDA with gas ionization detector has poor Li depth resolution but could be improved to 120×10^{15} atoms/cm^2 depth resolution by using a SSD energy detector and 30 MeV O ions under 67.5° gracing incidence. However, to get analyzable statistics in TOF-ERDA experiments in transmission/reflection geometry, beam damage is worse in battery even with He ions due to small solid angles and potentially poor sensitivity of time-of-flight detectors for light species. On the other hand, the coincidence ERDA experiment features good sensitivity with high Li depth resolution and low beam damage to the battery. Thus, the coincidence ERDA experiments provide promising pathways for *in-operando* depth profiling for Li and other light elements in thin film batteries. To further assess the capability of the investigated methodology, detailed studies of the flux and fluence dependence of detection limits, achievable time resolution, and sample degradation are highly desirable.

ACKNOWLEDGMENTS

Accelerator operation was supported by the Swedish Research Council VR-RFI (Contract Nos. 2017-00646_9 and 2019-00191) and the Swedish Foundation for Strategic Research (Contract No. RIF14-0053).

DATA AVAILABILITY

The data that support the findings of this study are available from the corresponding author upon reasonable request.

REFERENCES

[1]T. Tanabe, Phys. Scr. **T159**, 014044 (2014).
[2]R. Mohtadi and S.-I. Orimo, Nat. Rev. Mater. **2**, 16091 (2017).
[3]T. Liu, L. Lin, X. Bi, L. Tian, K. Yang, J. Liu, M. Li, Z. Chen, J. Lu, K. Amine, K. Xu, and F. Pan, Nat. Nanotechnol. **14**, 50 (2019).
[4]X. Wang, M. Zhang, J. Alvarado, S. Wang, M. Sina, B. Lu, J. Bouwer, W. Xu, J. Xiao, J.-G. Zhang, J. Liu, and Y. S. Meng, Nano Lett. **17**, 7606 (2017).
[5]Z. Ding, J. Li, J. Li, and C. An, J. Electrochem. Soc. **167**, 070541 (2020).
[6]D. H. S. Tan, A. Banerjee, Z. Chen, and Y. S. Meng, Nat. Nanotechnol. **15**, 170 (2020).
[7]E. Zhao, Z.-G. Zhang, X. Li, L. He, X. Yu, H. Li, and F. Wang, Chin. Phys. B **29**, 018201 (2020).

[8]D. Sheptyakov, L. Boulet-Roblin, V. Pomjakushin, P. Borel, C. Tessierc, and C. Villevieille, J. Mater. Chem. A **8**, 1288 (2020).
[9]S. Taminato, M. Yonemura, S. Shiotani, T. Kamiyama, S. Torii, M. Nagao *et al.*, Sci. Rep. **6**, 28843 (2016).
[10]A. Schwöbel, R. Hausbrand, and W. Jaegermann, Solid State Ionics **273**, 51 (2015).
[11]P. P. R. M. L. Harks, F. M. Mulder, and P. H. L. Notten, J. Power Sources **288**, 92 (2015).
[12]Y. Liu, N. S. Hudak, D. L. Huber, S. J. Limmer, J. P. Sullivan, and J. Y. Huang, Nano Lett. **11**, 4188 (2011).
[13]S. Surblé, C. Paireau, J.-F. Martin, V. Tarnopolskiy, M. Gauthier, H. Khodja, L. Daniel, and S. Patoux, J. Power Sources **393**, 37 (2018).
[14]B. Tsuchiya, J. Ohnishi, Y. Sasaki, T. Yamamoto, Y. Yamamoto, M. Motoyama, Y. Iriyama, and K. Morita, Adv. Mater. Interfaces **6**, 1900100 (2019).
[15]K. Morita, B. Tsuchiya, H. Tsuchida, and T. Majima, Solid State Ionics **344**, 115135 (2020).
[16]V. Mathayan, M. V. Moro, K. Morita, B. Tsuchiya, R. Ye, M. Baba, and D. Primetzhofer, Appl. Phys. Lett. **117**, 023902 (2020).
[17]F. A. Weis, L. Ros, P. Reichart, H. Skogby, P. Kristiansson, and G. Dollinger, Phys. Chem. Miner. **45**, 669 (2018).
[18]P. Reichart, M. Moser, C. Greubel, K. Peeper, and G. Dollinger, Nucl. Instrum. Methods Phys. Res. B **371**, 178 (2016).
[19]I. B. Radović, M. Jakšić, and F. Schiettekatte, J. Anal. At. Spectrom. **24**, 194 (2009).
[20]R. Ye, K. Ohta, and M. Baba, ECS Trans. **73**, 49 (2016).
[21]M. Mayer, AIP Conf. Proc. **475**, 541 (1999).
[22]Y. Serruys, J. Tirira, and P. Trocellier, *Forward Recoil Spectrometry* (Springer, 1996).
[23]J. Mayer and E. Rimini, *Ion Handbook for Material Analysis* (Academic Press, New York, 1977).
[24]P. Ström, P. Petersson, M. Rubel, and G. Possnert, Rev. Sci. Instrum. **87**, 103303 (2016).
[25]M. Mayer, Nucl. Instrum. Methods Phys. Res. B **266**, 1852 (2008).
[26]J. F. Ziegler, M. D. Ziegler, and J. P. Biersack, Nucl. Instrum. Methods Phys. Res. B **268**, 1818 (2010).
[27]V. Paneta, A. Kafkarkou, M. Kokkoris, and A. Lagoyannis, Nucl. Instrum. Methods Phys. Res. B **288**, 53 (2012).
[28]D. F. Fang, E. G. Bilpuch, C. R. Westerfeldt, and G. E. Mitchell, Phys. Rev. C **37**, 28 (1988).
[29]A. M. Bachmann, H. Brand, H. Freiesleben, Y. Leifels, K. W. Potthast, P. Rosenthal, and B. Kamys, Z. Phys. A: Hadrons Nucl. **346**, 47 (1993).
[30]L. L. Pinsonneault and J. M. Blair, Phys. Rev. **141**, 961 (1966).
[31]E. Norbeck, P. T. Wu, C. R. Chen, and R. R. Carlson, Phys. Rev. C **28**, 1140 (1983).
[32]M. Mayer, K. Arstila, K. Nordlund, E. Edelmann, and J. Keinonen, Nucl. Instrum. Methods Phys. Res. B **249**, 823 (2006).
[33]F. Schiettekatte, AIP Conf. Proc. **1099**, 314 (2009).
[34]H.-Y. Qu, D. Primetzhofer, M. A. Arvizua, Z. Qiu, U. Cindemir, C. G. Granqvist, and G. A. Niklasson, ACS Appl. Mater. Interfaces **9**, 42420 (2017).
[35]Z. Siketić, I. Bogdanović Radović, I. Sudić, and M. Jakšić, Sci. Rep. **8**, 10392 (2018).
[36]Y. Zhang, H. J. Whitlow, T. Winzell, I. F. Bubb, T. Sajavaara, K. Arstila, and J. Keinonen, Nucl. Instrum. Methods Phys. Res. B **149**, 477 (1999).
[37]J. Julin, M. Laitinen, and T. Sajavaara, Nucl. Instrum. Methods Phys. Res. B **332**, 271 (2014).
[38]S. Möller, T. Satoh, Y. Ishii, B. Teßmer, R. Guerdelli, T. Kamiya, K. Fujita, K. Suzuki, Y. Kato, H.-D. Wiemhöfer, K. Mima, and M. Finsterbusch, Batteries **7**, 41 (2021).
[39]M. Moser, P. Reichart, A. Bergmaier, C. Greubel, F. Schiettekatte, and G. Dollinger, Nucl. Instrum. Methods Phys. Res. B **371**, 161 (2016).